Li, Jianfeng and Agyakwa, Pearl and Evans, Paul and Johnson, Christopher Mark and Zhao, Yimin and Wu, Yibo and Evans, Kim (2014) Packaging/assembling technologies for a high performance SiC-based planar power module. In: Greener Aviation Conference 2014: Clean Sky Breakthrough and Worldwide Status, 12-14 March 2014, Brussels, Belgium.

Packaging / Assembling Technologies for a High Performance SiC-Based Planar Power Module

Jianfeng Li, Pearl Agyakwa, Paul Evans, Christopher Mark Johnson
Department of Electrical and Electronic Engineering, The University of Nottingham, University Park, Nottingham NG7 2RD, United Kingdom

Yimin Zhao, Yibo Wu, Kim Evans
Dynex Semiconductor Limited, Doddington Road, Lincoln LN6 3LF, United Kingdom

This work is to investigate the relevant packaging / assembling technologies for developing a SiC-based planar power module which is aimed to meet the requirements such as operating temperature of -60 ºC to 200 ºC, SiC devices connected to 540 V DC bus and non-hermetic module. The results reported in this paper include: (i) design of a compact wire-less SiC-based power module with low parasitic inductance; (ii) demonstrated feasibility and reliability for the sintering of Ag nanoparticles and flexible printed circuit board as alternative joining and interconnect technologies which have been selected to assemble the designed power module; and (iii) preliminary construction of the designed module and electrical switching test of the constructed module.

INTRODUCTION

In a conventional power module as shown in Fig. 1, solder joints are used to attach Si or SiC devices (chips) and bus bars on the ceramic-based substrate with Cu circuit conductor, and bond the substrates to the base-plate or cooler. Wire bonds in combination with the bus bars are used to achieve the interconnections. However, the eutectic or near eutectic Sn-Ag and Sn-Ag-Cu solders that are commonly used for power device attachments are not reliable at temperatures above 125 °C [1]. This is because they are prone to creep at elevated temperatures and the accumulation of plastic work leads to crack initiation and propagation [2,3]. Also, wire bonds have limited ability to dissipate heat and have relatively high parasitic inductance which often restricts the thermal and electrical performance of the power modules [4,5].

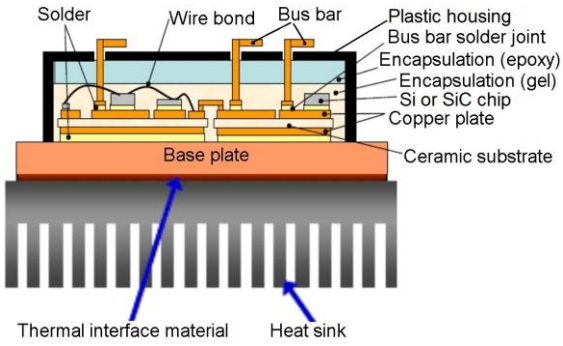

Fig. 1. Schematic diagram of a conventional power module.

With the advances in power devices and the movement toward new energy technology and low carbon economy, there is an increasing demand in the development of innovative power electronics with increased power densities, high reliability in harsh environments and higher levels of integration and low electromagnetic emission. For example, SiC power devices have been developed rapidly and can be packaged into power modules with high power densities and operated at temperatures of over 200 °C, and even up to 500°C [6-8]. The present work is to develop an innovative compact SiC-based planar power module for aerospace application. In particular, the developed power module is aimed to meet the requirements such as operating temperature of -60 ºC to 200 ºC, SiC devices connected to 540 V DC bus and non-hermetic module.

The conventional packaging and assembling technologies based on the Sn-based solder joints and Al wire bonds cannot meet the above requirements. To overcome this problem, a SiC-based planar power module to target the application requirements has been designed, and the selected packaging / assemblies technologies have been investigated. This paper will start with the design of the power module with the consideration of joining and interconnect technologies. Then it will place emphasis on the sintering of Ag nanoparticles which has been selected as the joining technology for assembling the designed power module. The results obtained from this section can be used to justify the selection of this joining technology and determine the sintering parameters for assembling the designed power module. After this, it will introduce the preliminary construction of the designed power module, and the electrical switching test of the constructed module. Finally, it will draw the conclusions and point out further work based on all the results obtained.

DESIGN OF THE POWER MODULE

Consideration of joining technology

The standard approach for improving the solder joint reliability of high temperature electronics is the use of high-lead solders, such as Pb2SnAg2.5 [1,9]. However, EU environmental legislation is set to remove lead from most solder applications due to toxicity issues. In addition, these high-lead solder joints can be prone to strain hardening and eventual crack formation resulting in loss of electrical continuity [3,10]. Au-based off-eutectic solder is another type of alloy that have been used for many years in high temperature electronics. However, this type of solder is cost-ineffective, has poor solderability, and may produce some Au-rich AuSn phases that are brittle leading to early failure [9,11].

To address the increasing challenge of reliability problems for solder alloys to be used in power device attachments for high temperature and high reliability applications, several alternatives have been proposed and under intensive investigation. They include sintering of Ag particles and nano-particles [12,13], transient liquid phase (TLP) soldering [14,15], liquid solder joint [16], local brazing [17], nano-particle reinforced solders [18], and several emerging solder alloys [19,20]. Generally speaking, powder-based TLP soldering and the emerging solder alloys are more compatible with the conventional solder reflow process. The other materials and processes may be more attractive, but require some modification or complementation to the conventional solder reflow process.

The improvement in reliability by using nanoparticle reinforced solders is limited [18]. The emerging solder alloys such as Bi-based and ZnAl-based solder alloys have to be reflowed at relatively temperatures and have poor spreadability and solderability [19,20]. Both plating / foil-based TLP soldering and liquid solder joint require thickening and /or modification of contact metallization on the semiconductor devices [15,16]. The nanostructured reactive Al/Ni foils used in local brazing were prepared using sputtering process, and hence very expensive [17]. There are no robust reliability data that have been reported for the powder-based TLP joints and local-brazed joints for power die attachments. By contrast, the sintering of Ag nanoparticle can be carried out on the semiconductor devices with the common Ni/Ag or Ni\Au contact metallization. Also, there is a wealthy of data which were reported and demonstrated the reliability of sintered Ag joints for high-temperature applications [12,13,21-23]. Therefore, in the present design, the sintering of Ag nanoparticles is selected as the joining technology.

It should be pointed out that pressure-less sintering of Ag nanoparticles had been demonstrated on 1.706mm×1.380 mm and 3mm×3mm SiC devices [21,22]. However, in this approach, it is extremely important to hold and manually smear the devices around 1-2 mm on the printed wet Ag nanoparticle paste for ensuring 100% initial contact [21,22]. As a result, this approach cannot be used in the present power module because any smearing of the devices on the wet paste would lead to misalignment and short circuit between the source and gate of the devices. Therefore, it is the pressure-assisted sintering of Ag nanoparticles which has been selected as the present joining technology.

Consideration of interconnect technology

To improve the ability of dissipating heat and reduce the parasitic inductance in conventional power modules, several replacements of wire-bonds, such as ribbon-bond [4], dimple array [5], embedded chip technology [24], silicon interposer [25], solder bump [26], metal bump [27,28] and press-pack bus-bar-like interconnects [29] were proposed and investigated over the past years. These were mainly done on Si devices, and there is a lack of data on the reliability and large-scale manufacturability for the implementation of these technologies. In comparison with Si devices, it is more difficult to implement these interconnect technologies on SiC devices because of much smaller device features. In the present design, flexible PCB is considered to replace both the wire bonds and bus bars in the conventional power modules. Such an approach making use of the well-developed and sophisticate PCB technology can be employed to easily achieve the spatial resolution to contact SiC device features.

Structural design of the power module

A full SiC and wire-less half-bridge power switch module has been designed based on the Ag sintering and flexible PCB technologies. The designed module has a compact structural volume of 54 mm × 53 mm × 10 mm. The Si_3N_4-based substrate accommodating the SiC devices is underneath the flexible PCB. The flexible PCB is fixed on a plastic frame. Screws and auxiliary pins are used to fix the flexible PCB and connect to external supply, load and gate signals. As shown in Fig. 2, a plastic lid with pillars containing springs is used to further isolate the components and reinforce the thermal contact of the Si_3N_4-based substrate to a cold plate or cooler.

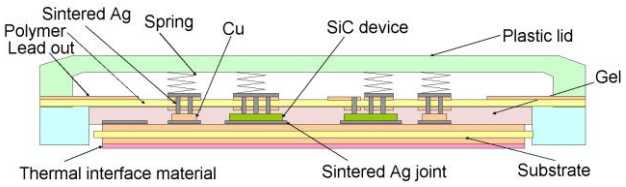

Fig. 2. Cross-sectional views of the designed power module.

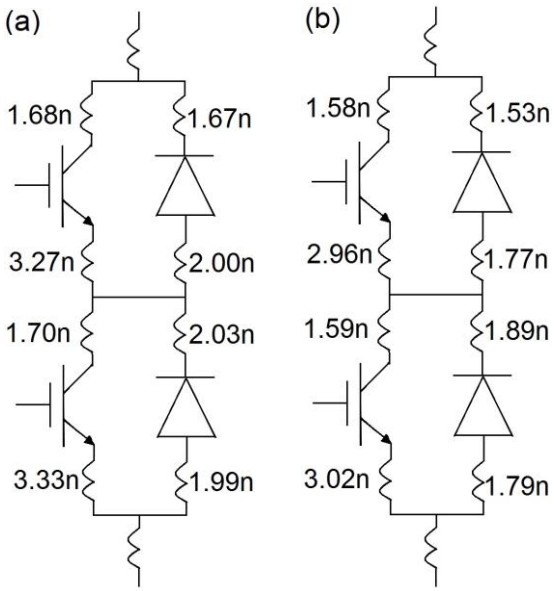

Fig. 3. Equivalent circuit with extracted inductances in the designed power module at: (a) 1 kHz, (b) 100 kHz.

The substrate is populated with 8 SiC devices include 4 SiC junction gate field-effect transistors (JFETs) and 4 SiC Schottky diodes which can be selected from 600 V to 1700 V. As aforementioned, the sintering of Ag nanoparticles has been selected as the joining technology for the assembling process. The sintered Ag joints will be used to join the front sides of both the SiC devices and Cu conductive supports to the bottom metal layer of the flexible PCB, and join the back sides of both the SiC devices and Cu conductive supports to the Si_3N_4-based substrate. The substrate, flexible PCB and SiC die are all plated with Ag or Au. The gap between the substrate and flexible PCB will be filled with insulating silicone gel.

Because of the elimination of conventional wire-bonds and bus-bars, such a designed power module is expected to have extremely low parasitic inductance and hence improved electrical performance. Fig. 3 gives the parasitic inductance values extracted with the FastHenry. It can be seen that the extracted values are indeed extremely low.

SINTERING OF SILVER NANOPARTICLES

Effects of sintering parameters

Unlike solder reflow where solder joints are formed through liquid wetting, solid-liquid interfacial reaction and solidification, sintering is an atomic diffusion processing where the bonding is accomplished through atomic diffusion and particle consolidation. There are re-arrangement of Ag nanoparticles, densification and reduction in porosity and grain growth occurring during the sintering process. The microstructure and hence the thermal and electrical performance as well as thermo-mechanical reliability of the sintered Ag joints are sensitive to both the formulation of the paste and the sintering parameters such as heating rate, sintering temperature, pressure and time. Therefore, it is important to understand the effects of these parameters for selecting the suitable sintering conditions.

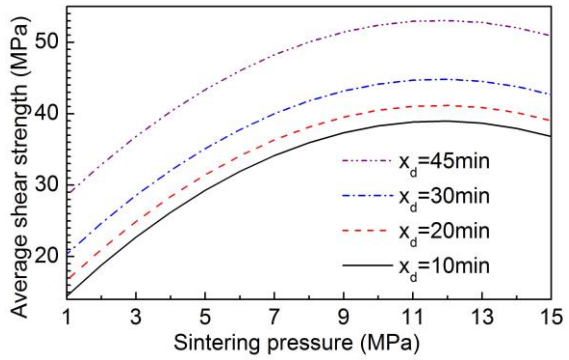

Fig. 4. plots of average shear strength versus sintering pressure for sintering temperature of 250 °C and 4 times, t_d, of drying the printed paste at 130 °C.

Shear strengths of the sintered Ag joints were commonly used as feedbacks for rapid selection and/or optimization of the sintering parameters [21,31]. Using the same paste of Ag nanoparticles and customer-made sintering press as used in the present work, the effects of the sintering parameters on the shear strength of the sintered Ag joints of attaching multiple SiC devices were systematically investigated. The details have been reported elsewhere [32], and are not repeated here. Briefly speaking, the sintering parameters investigated were: drying the printed paste of Ag nanoparticles at 130 ºC, sintering temperature of 240 to 300 ºC, and sintering pressure of 1 to 15 MPa. The results indicated that the effect of the sintering time on the average shear strength of the multiple device attachments is negligible. The average shear strength increases with increasing the time of drying the printed Ag paste at 130 ºC and decreasing the sintering temperature. At lower sintering temperature and pressure, the average shear strength rapidly increases with increasing the pressure. At higher sintering temperature and pressure, the average shear strength slightly decreases with increasing the pressure. Fig. 4 shows a few derived plots describing the effects of sintering parameters on the average shear strength of multiple device attachments and can be used to determine and discuss the sintering parameters used in the present work.

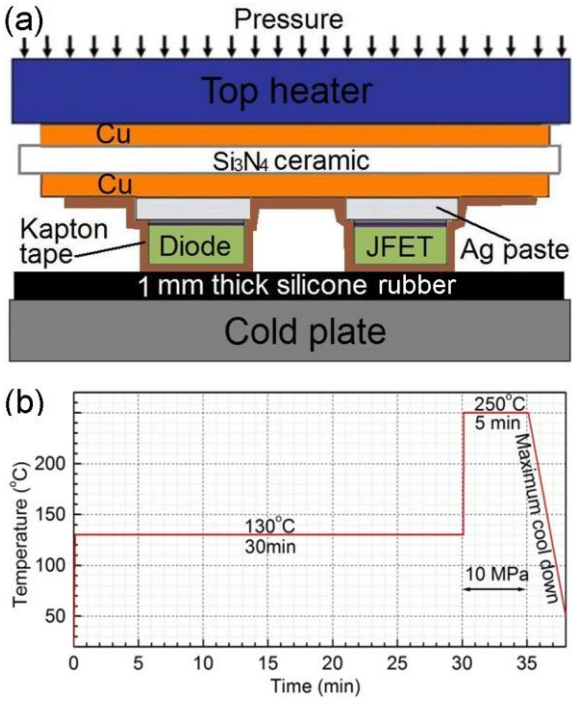

Fig.5. Schematic description of the sintering process to attach the SiC devices on the substrate for the thermal cycling test: (a) cross section of the sample; (b) temperature and pressure profile.

Thermo-mechanical reliability of device attachment

In order to do this test, a SiC JFET and a SiC diode were attached to a Si_3N_4-based substrate by Ag sintering. The surface finish on the as-received Si_3N_4-based substrate was NiP, and an additional Ag layer was deposited with brush plating on top of the NiP finish. During the preparation of the sample, a layer of 100 μm-thick paste of Ag nanoparticles was first applied on the Si_3N_4-based substrates by stencil printing, (followed by drying the paste at 130 °C for 30 minutes). One SiC JFET and one SiC diode were placed on the dried paste and fixed with Kapton tape. The sample was then turned upside down and put on 1 mm thick silicone rubber situated on the cold plate of the sintering press, see Fig. 5. The sintering was performed at 250 ºC and 10 MPa for 5 minutes, before releasing the pressure and cooling the sample down to room temperature (within 3 minutes).

From Fig. 4, the sintered device attachments using the sintering parameter shown in Fig. 5 are expected to have an average shear strength higher than 40 MPa. Fig. 8 presents the scanning electronic microscopy (SEM) images taken from the cross-section of the as-sintered sample of attaching one SiC JFET using the same sintering parameter. The sample had been etched prior to SEM observation using plasma cleaning to remove the top layer on the polished cross section to reveal the pores and interfacial bonding in the sintered Ag joint. It can be seen that the thickness and microstructure of the sintered Ag joint are quite uniform along the entire cross section. Using the image analysis method descried in the previous

work [32], the porosity of the sintered Ag layer measured from Fig. 6b is 9.8%. The pores which can be observed from this SEM image are in the range of 0.02 μm to 0.25 μm in size.

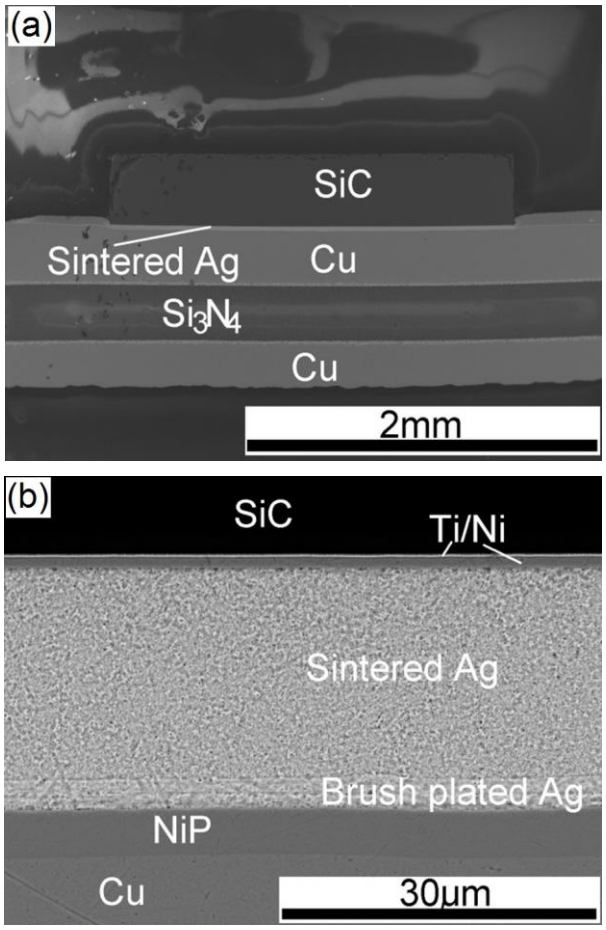

Fig. 6. SEM images taken from the cross section of one as-sintered sample: (a) overview; (b) enlarged view.

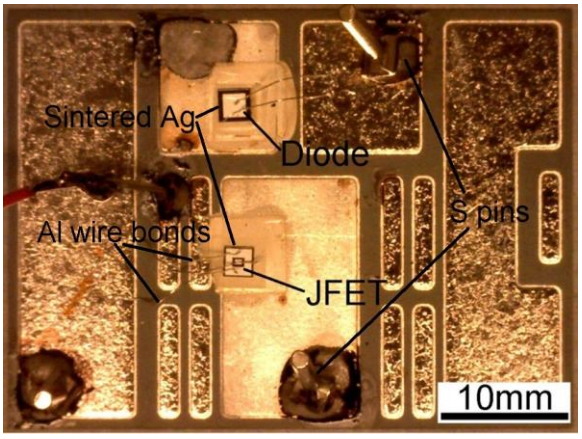

Fig. 7. Photograph taken from the as-prepared sample for the thermal cycling test.

For the purpose of comparison, a similar substrate with Pb5Sn solder joints was also prepared using the reflow profile as detailed in a previous work [33]. After attaching the SiC devices, Al wires bonds and S pins were also bonded on the substrates to form a mechanical structure similar to those in a realistic conventional power module, see Fig. 7. The Al wire bonds were made using ultrasonic bonding, and the S pins were manually soldered on the substrate with Pb95Sn solder wire at a temperature of 350 ºC. Then the samples were put into an environmental chamber temperature cycled from -60 ºC to 200 ºC to test their thermo-mechanical reliability.

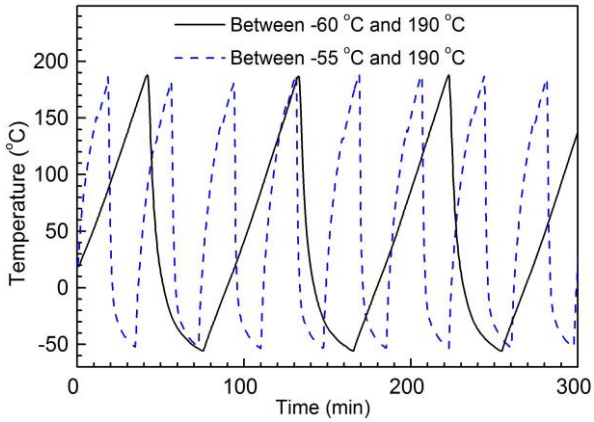

Fig. 8. Temperature profiles measured from the sample during thermal cycling.

The thermal cycling was initially carried out in a relatively large environmental chamber. Using a K-type thermocouple one representative sample/substrate, the cycling temperature was measured between -60 ºC and +190 ºC as shown in Fig. 9. After 250 thermal cycles, testing continued in another environmental chamber and the temperature measured the sample/substrate was frombetween -55 ºC and 190 ºC (also shown in Fig. 8). The structural integrity of the samples before and after different periods of thermal cycling; in particular the initiation and growth of voids/defects in both the sintered Ag joints and the Pb5Sn solder joints of attaching the SiC devices, have been characterised with three-dimensional X-ray computed tomography (CT) imaging, carried out on an Xradia Versa XRM-500 system. The percentags of voids/defects in both joints have been calculated from the reconstructed X-ray CT images.

In the as-sintered Ag joints attaching the SiC devices, no appreciable void/defect was detected using the X-ray CT imaging under a resolution of ~ 2 μm. By contrast, there was an average of 6.5% for the percentage of voids/defects in the as-reflowed Pb5Sn solder joints. These voids/defects were approximately round pores and 10 μm to 300 μm in diameter. During the thermal cycling, formation and growth of interconnected and networked cracks which were mainly in parallel with the through-thickness direction in both the sintered Ag joints and the Pb5Sn solder joints were detected. Fig. 9 shows the reconstructed X-ray CT images obtained from the samples after 2000 thermal cycles. Fig. 10 further presents the evolution curves of percentags of voids/defects in both joints of attaching the SiC devices with respect to number of thermal cycles. Each of the two curves is the average of the results obtained from the two joints of attaching two SiC devices on the same Si_3N_4-based substrate. Provided that the increase in the percentage of voids/defects is used as a criterion to assess the degradation of the joints, it can be seen that under 640 cycles, the degradation rate of the sintered Ag joint is much slower than that of the standard Pb5Sn solder joint. Over 640 cycles, degradation rate of the sintered Ag joint is similar to that of the standard Pb5Sn solder joint. As a whole, the sintered Ag joint appears to be more reliable than the Pb5Sn solder joint.

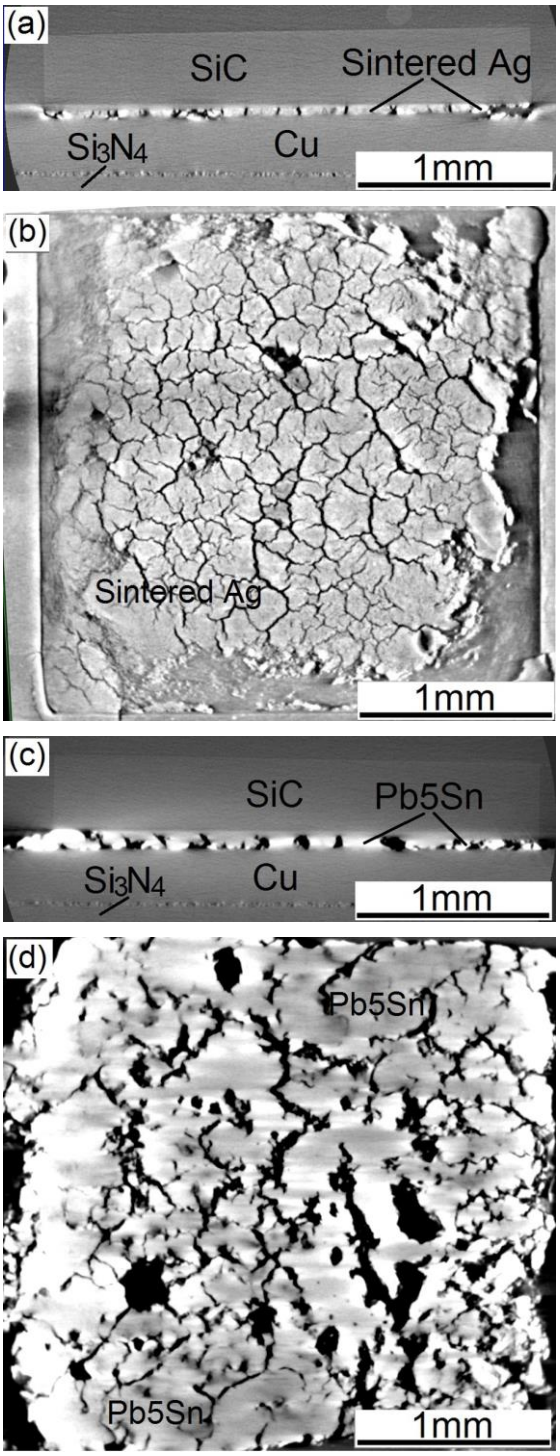

Fig. 9. Reconstructed X-ray CT images obtained from: (a) one sintered Ag joint, x-z cross section, (b) the same sintered Ag joint, x-y plane; (c) one Pb5Sn solder joint, x-z cross section; (d) the same Pb5Sn solder joint, x-y plane, after 2000 cycles of therml cycling.

Feasibility / reliability of bonding flexible PCB

The feasiability of bonding flexible PCBs was initially investigated on Si devices with 0.5/0.3 μm thick NiP/Pd on their front sides and 0.3 μm thick Ni/Ag on their back sides which are both suitable for the Ag sintering technology. These Si devices were 10×9.5×0.07 mm insulated gate bipolar transistors (IGBTs) and 9.5×5.5×0.07 mm diodes. The flexible PCB consisted of polyimide (25um in thickness) with Cu features (~30μm in thickness and with 0.1 μm thick Ag finish) on both sides, and vias of 0.6 to 1 mm in diameter through all the polyimide layer and both Cu feature layers. The substrates used included both Si_3N_4-based substrate (0.3/0/32/0.3 mm thick Cu/Si_3N_4/Cu and 5/0.1 μm thick NiP/Ag finish), and AlN-based substrate (0.3/1/0.3 mm thick Cu/AlN/Cu and 5/0.1 μm thick NiP/Au finish). Experimets were succssful in assembing PCB/diode/substrate, PCB/IGBT /substrate and substrate/PCB/IGBT/substrate samples.

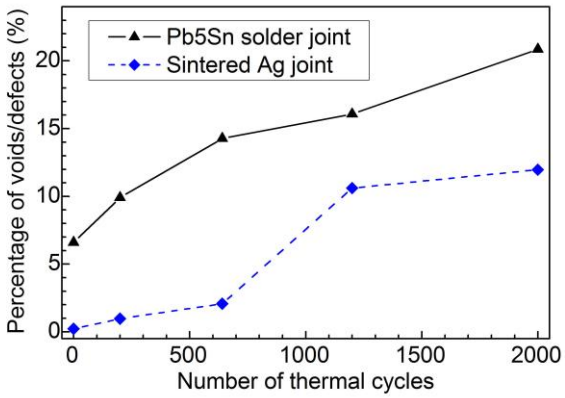

Fig. 10. Plots of percentags of voids/defects versus number of thermal cycles, for the joints of attaching the SiC devices during thermal cycling test.

As one example, the assembling process of preparing one PCB/diode/substrate sample is briefly described as follows. First, 100 μm thick paste of Ag nanoparticles was applied on the top surface of ~30 μm thick Cu with 0.1 μm thick Ag finish which was laminated on 25 μm thick polyimide, and dried at 130 °C for 30 min. Then a piece of flexible PCB consisting of polyimide (25 μm in thickness) with Cu features (~30 μm in thickness and with 0.1 μm thick Ag finish) on both sides, and 8 through vias (1 mm in diameter) was placed on the top of the dried Ag paste. Following this, another layer of paste of Ag nanoparticles was applied on the top and filled into the through vias of the flexible PCB by using a mask of 100 μm in thickness and with an opening of 9.5 mm by 5.5 mm, and dried at 130 °C for 30 min. At the same time, a layer of 100 μm thick paste of Ag nanoparticles was applied on one substrate with 5/0.1 μm thick NiP/Au finish and also dried 130 °C for 30 min. Once all the above components were ready, they were placed together and fixed with kapton tape, and then put on a ϕ60×5 mm Al disc supported by 5 mm thick cured silicone rubber on the bottom cold plate of the sintering press, as schematically shown in Fig. 11. The final sintering was carried out by dropping the top heater of the sintering press at 260 °C immediately to a pressure of ~5 MPa for 5 minutes, before releasing the pressure and cooling the sample down to room temperature (within 3 minutes).

Figure 12a shows an optical microscopy (OM) image taken from the polished cross section of the sample prepared with the schematica geometry shown in Fig. 11. It can be seen that the sintered Ag well filled in the through via of the flexible PCB, while also joined to both sides of the diode, the top substrate and the bottom ~30 μm thick Cu laminated on 25μm thick polyimide (this layer polyimide is invisible in Fig. 12a). Note that the bottom Cu in Fig. 12a is not flat, and this may be related to the different deformation and/or thermal

expansion/contract between the polyimide and sintered Ag layers during the sintering process. If the bottom ~30 μm thick Cu laminated on 25 μm thick polyimide in Fig.11 was replaced with a piece of Kapton adhesive tape, the bonding of the sintered Ag joints to the side wall of through via of the flexible PCB became poor (Fig. 12b). This may be ascribed to a kind of "repelling force" caused by the de-wetting of the sintered Ag to the Kapton adhesive tape during the sintering process.

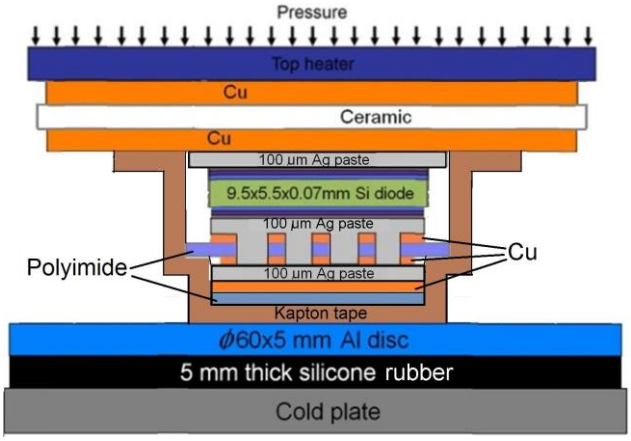

Fig. 11. Schematic sample geometry for assembling the Cu/PCB/diode/substrate sample.

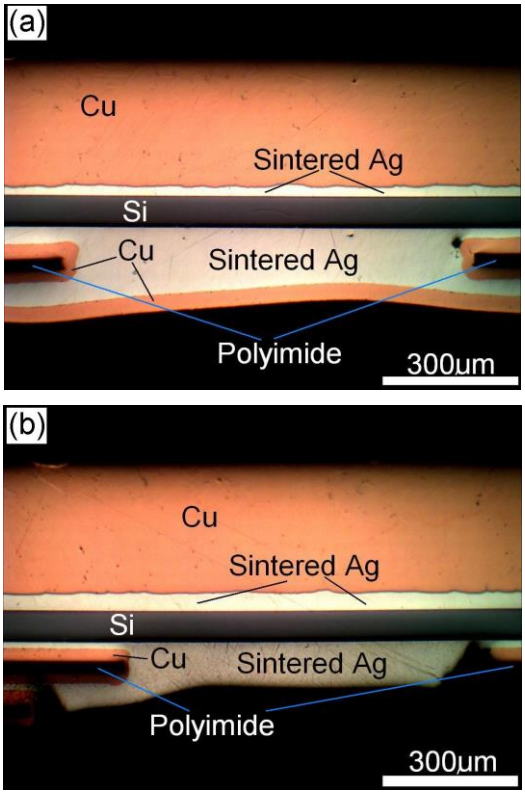

Fig. 12. OM images takne from the polished cross sections of the assembled: (a) Cu/PCB/diode/substrate sample; (b) Kapton/PCB/diode/substrate sample.

The reliability of bonding the flexible PCB on the front side of the 9.5×5.5×0.07 mm Si diode was also tested under power cycling. For preparing the samples in this test, the substrate used was the AlN-based substrate with NiP/Au finish. The flxeible PCB was laminated with Cu on both sides and the Cu plated with a Au flash layer. There were 10 through vias of 1 mm in diameter at one end of the flexible PCB which was bonded on the front side of the Si diode, and 6 through vias of 1.5 mm in diameter at the other end of the flexible PCB which was bonded on a 9.5×5.5×0.07 mm Cu support with Ag finish.

Figure 13 shows one represenattive sample prepared for the power cycling test. During preparing this type of sample, one piece of the flexible was first placed and fixed on a piece of 25 μm thick Ag foil with the same size. This is to blind the vias on one side of the flexible PCB and improve the bonding of the sinterd Ag layer to the side walls of the vias. Based on the result shown in Fig. 12, this is necessary to ensure good bonding of the sintered Ag to the side walls of the through vias. Then 100 μm thick paste of Ag nanoparticles was applied on the top and filled into the through vias of the flexible PCB by using a 100 μm thick mask with two openings of 9.5 mm by 5.5 mm, and dried at 130 °C. At the same time, a layer of paste of Ag nanoparticles was also applied on the the substrate by using a 100 μm thick mask with two openings of 11 mm by 7 mm, and dried 130 °C. Following this, one Si diode and one Cu support were placed on the dried paste on the substrate, and then the flexible PCB with dired paste was aligned and put on the front side of the Si deiode and Cu support. All the components were further fixed with kapton tape, and then put on a ϕ60×5 mm Al disc supported by 5 mm thick cured silicone rubber on the bottom cold plate of the sintering press. The final sintering was carried out by dropping the top heater of the sintering press at 250 °C immediately to a pressure of ~5 MPa or ~ 10 MPa for 5 minutes, before releasing the pressure and cooling the sample down to room temperature (within 3 minutes).

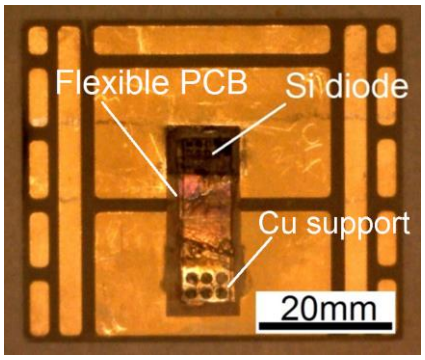

Fig. 13. Photography of one as-prepared sample for the power cycling test.

Power cycling tests were carried out between 40 °C and 120 °C by passing current through the diodes with cooling being applied throgh a water-based cold plate. The time for one cycle was in the range of 5 to 9 seconds. Typical duty cycles, i.e. the ratios of heating time to cycle time, were 30% to 50%. As presented in Fig. 14, the failure of any sample was reflected by the significant increase in the forward voltage of the diode bonded in the sample. When taken as a whole, the sintered samples have a longer lifetime than the Al wire-bonded samples and the samples prepared under 10 MPa are more reliable than those samples prepared under 5 MPa. In particular, the samples prepared using the sintering of Ag nanoparticles under 10 MPa display a much longer lifetime than the conventional Al wire bonded samples.

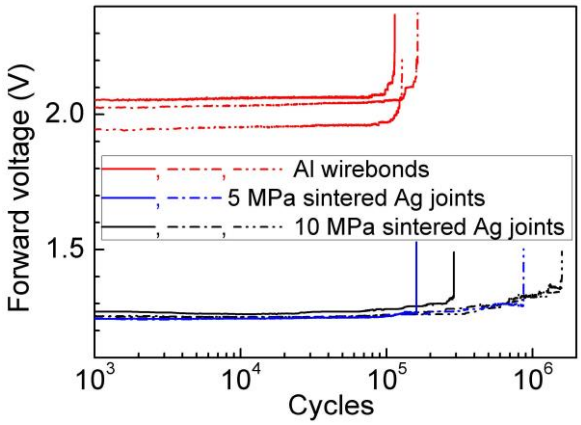

Fig. 14. Evolution of forward voltages versus cycles for the Si diode under the power cycling tests.

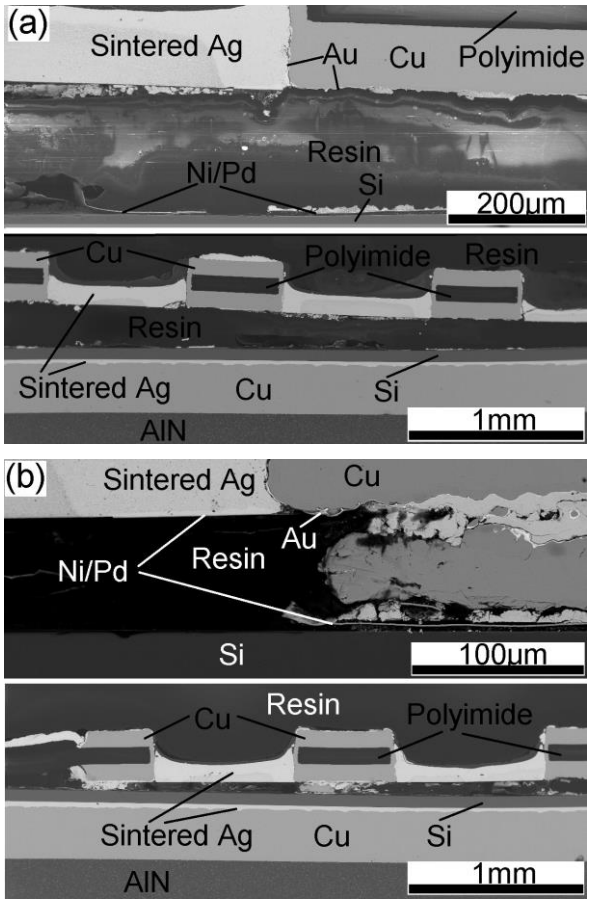

Fig. 15. SEM images taken from the polished cross sections of the samples after power cycling test: (a) 289,211 cycles; (b) 1,682,211 cycles.

The samples failed after the power cycling tests were cross sectioned and polished for SEM observation. No similar interconnected and networked cracks were observed within the sintered Ag layers after the power cycling tests. This can be ascribed to the peak temperature of 120 °C during the power cycling which is lower than the peak temperaure of 190 °C during the thermal cycling. In all the samples with lifetimes shorter than 400k cycles, the failure occurred at the interface between the sintered Ag layer and the Ni/Pd finish on the front sides of the Si diodes (Fig. 15a). In all the samples with lifetimes longer than 400k cycles, the failure mainly occurred at the interface between the Ni/Pd finish and the Si on the front sides of the Si diodes, and the NiP/Pd had partly been moved to the de-bonded sintered Ag layer (Fig. 15b). Such results demonstrate that a certain level of pressure is necessary during the sintering process to improve the bonding strength for achieving highly reliable sintered Ag joints of bonding the flexible PCB. Improvement in the bonding strength of the NiP/Pd finish is required if further improved reliablity of the sintered Ag joints of bonding the flexible PCB is needed.

These results demonstrate the feasibility of bonding the flexible PCB to the front sides of the semiconductor devices with suitable finishes, and a higher pressure is necessary to achieve a more reliable sintered Ag joint. Similar failure mechanisms can be expected if the flexible PCB proposed in the designed power module was used to assemble the samples for the power cycling tests. This is because the two types of failure observed in Fig. 14 both occurred at the front side of the semiconductor device, and are not related to the bonding of the sintered Ag to the side walls of the through vias in the flexible PCB.

Construction and Switching Test

Construction of the designed module

Both manual and automatic assembling processes can be developed to construct the designed power module. Thus far, a manual assembling process has been considered, and consists of joining the SiC devices and Cu conductive supports between the substrate and flexible PCB with the Ag sintering technology, attaching the sintered sample on the plastic frame, injecting insulating silicone gel to fill the gap between substrate and flexible PCB, and fixing the plastic lid to finalize the module. Because of the delay in obtaining the ordered plastic frame and lid parts, only the assembling experiment for joining the SiC devices and Cu conductive supports between the substrate and flexible PCB has been carried out.

A proper sintering jig was designed for fabrication of the double-side sintered module. The die positions and alignment to the substrate and PCB was defined by the sintering jig. After finishing the sintering process, the SiC devices had been joined between both the substrate and the flexible PCB. The sample was removed from the jig for the subsequent assembling process. Once the plastic frame and lid parts are received, the subsequent assembling experiments including attachment of plastic frame, injection of silicone gel and fixing of plastic lid will also be investigated.

Switching test of the as-sintered sample

The electrical switching performance of the as-sintered sample has been tested with a double pulse tester. Because no insulating silicone gel was filled in the gap between the substrate and flexible PCB, the maximum voltage of 400 V and current of 15 A have been applied during the test.

Fig. 16 is the schematic test circuit, and Fig. 10 presents the switching waveforms tested at 400 V and 15 A. It can be seen that the as-sintered sample can achieve the electrical function of switching on and switching off. However, the oscillation is significant and the switching time, in particular, the switching on time is quite long. Such a switching result is probably because of a slow gate

driving signal and the inductance existing in the gate driving loop. A new gate-drive circuit, optimised for high speed SiC JFETs is being designed and constructed to rectify this problem. It will be used to test both the as-sintered samples and the will-be fully assembled modules.

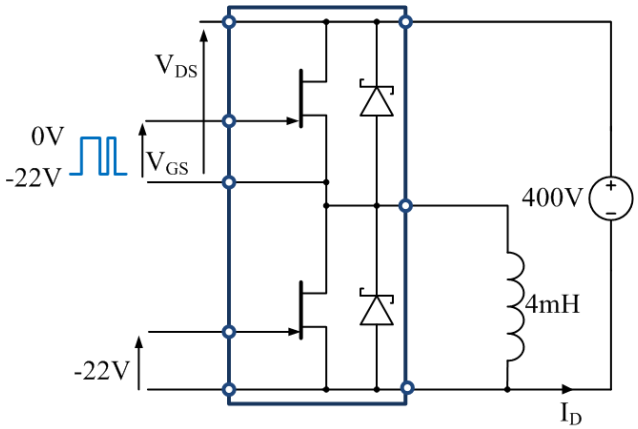

Fig. 16. Schematic circuit of the double pulse test.

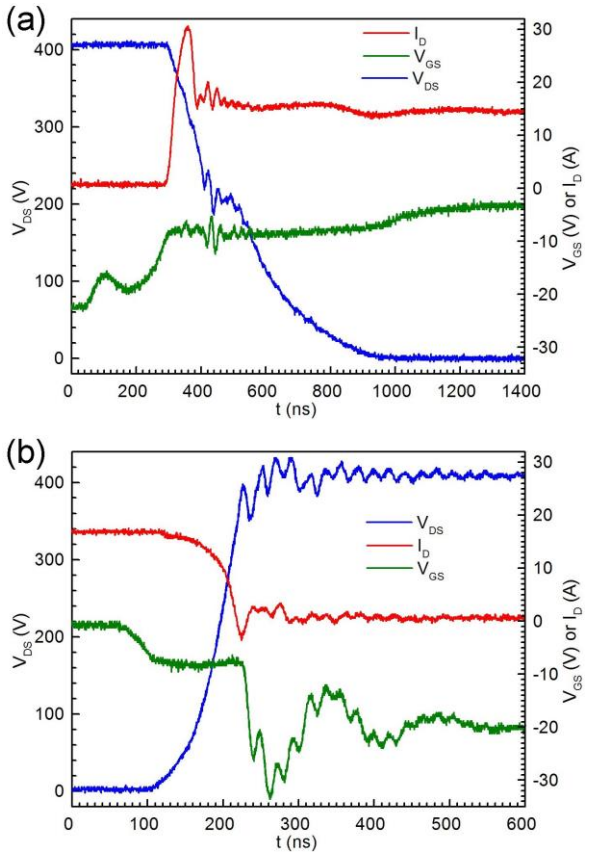

Fig. 17. Switching waveforms at 400 V and 15 A: (a) switching on waveforms; (b) switching off waveforms.

CONCLUSIONS AND FURTHER WORK

From all the above results obtained, the following conclusion can be drawn:

1) A compact full SiC and wire-less half-bridge power switch module aimed for aerospace application has been designed .based on the sintering of Ag nanoparticles and flexible PCB as joining and interconnect technologies.
2) Using appropriate sintering parameters, the sintered Ag joints can be more reliable than Pb5Sn solder joints for attaching SiC devices for high-temperature applications, e.g. aerospace application.
3) Using appropriate sintering parameters and contact metal finish on the front sides of semiconductor devices, the sintered Ag joints of bonding flexible PCB as alternative interconnect technology can also be more reliable than the conventional Al wire bonded interconnects.
4) A preliminary experiment demonstrates that the designed power module can be assembled with the Ag sintering technology and achieve the stacked integration with the electrical function of switching on and switching off.
5) Further work will be carrying on to finalize and optimize the assembling process for constructing the entire module, improve the gate-drive design to get better switching results, and test the electrical performance and thermo-mechanical reliability of the fully constructed module samples.

ACKNOWLEDGEMENTS

The authors gratefully acknowledge the support of the European Commission through the Seventh Research Framework Programme, CleanSky “Systems for Green Operations”. The authors wish to thank Oscar Khaselev and Mike Marczi of Cookson Electronics for providing the paste of Ag nanoparticles.

REFERENCES

[1] S.H. Mannan, M.P. Clode, *IEEE Transactions on Advanced Packaging* (2004), 27(3), 508-514.
[2] P.T. Vianco, J.A. Rejent, A.C. Kilgo, *Journal of Electronic Materials* (2004), 33(11), 1389-1400.
[3] C.M.L. Wu, D.Q. Yu, C.M.T Law, et al, *Materials Science & Engineering, R: Reports* (2004), R44(1), 1-44.
[4] C. Luechinger, in *Proceedings of 9th Electronics Packaging Technology Conference*, December 10-12, 2007, Singapore, pp. 47-54.
[5] G.Q. Lu, X. Liu, S. Wen, et al, *Soldering and Surface Mount Technology* (2004), 16(2), 27-40.
[6] P.G. Neudeck**,** *Institute of Physics Conf. Series 141: Compound Semiconductors* (1994), 1-6.
[7] Y. Sugawara, *Japanese Journal of applied Physics* (2004), 43, 6835-6847.
[8] J. Rabkowski, D. Peftitsis, H. Nee, *IEEE Industrial Electronics Magazine* (2012), 2 (2), 17-26.
[9] P.O. Quintero, F.P. McCluskey, *IEEE Transactions on Device and Materials Reliability* (2011), 11(4), 531-539.
[10] K. Zeng, K.N. Tu, *Materials Science & Engineering, R: Reports* (2002), R38(2), 55-105.
[11] S. Tabatabaei, A. Kumar, H. Ardebili, et al, *Microelectronics Reliability* (2012), 52(11), 2685-2689.
[12] Z. Zhang, G.Q. Lu, *IEEE Transactions on Electronics Packaging Manufacturing* (2002), 25(4), 279-283.
[13] E. Ide, S. Angata, A. Hirose, et al, *Acta Materialia* (2005), 53(8), 2385-2393.
[14] E.F. Lugscheider, S. Ferrara, *Advanced Engineering Materials* (2004), 6(3), 160-163.
15] J.F. Li, P.A. Agyakwa, C.M. Johnson, *Journal of*

Electronic Materials, http://link.springer.com/article/10.1007%2Fs11664-013-2971-7.
[16] J.F. Li, S.H. Mannan, M.P. Clode, et al, *Acta Materialia* (2007), 55(15), 5057-5071.
[17] J. Wang, E. Besnoin, A. Duckham, et al, *Applied Physics Letters* (2003), 83(19), 3987-3989.
[18] M. Amagai, *Microelectronics Reliability* (2008), 48(1), 1-16.
[19] Y. Takaku, K. Makino, K. Watanabe, et al, *Journal of Electronic Materials* (2009), 38(1), 54-60.
[20] Y. Takaku, I. Ohnuma, Y. Yamada, et al, *Journal of ASTM International* (2011), 8(1), 1-18.
[21] J.G. Bai, G.Q. Lu, *IEEE Transactions on Device and Materials Reliability* (2006), 6(3), 436-441.
[22] J.G. Bai, J. Yin, Z. Zhang, et al, *IEEE Transactions on Advanced Packaging* (2007), 30(3), 506-510.
[23] S. Kraft, A. Schletz, M. Marz, in *Proceedings of 7th International Conference on Integrated Power Electronics Systems*, March 6-8, 2012, Nuremberg, Germany, pp. 439-444.
[24] N. Zhu, J.D. van Wyk, Z. Liang, et al, *IEEE Transactions on Industry Applications* (2005), 41(6), 1603-1611,.
[25] N. Khan, S.W. Yoon, A.G.K. Viswanath, et al, *IEEE Transactions on Advanced Packaging* (2008), 31(1), 44-50.
[26] J.N. Calata, J.G. Bai, X. Liu, et al, *IEEE Transactions on Advanced Packaging* (2005), 28(3), 404-412.
[27] C.M. Johnson, C. Buttay, S.J. Rashid, et al, in *Proceedings of the 19th International Symposium on Power Semiconductor Devices & ICs*, May 27-30, 2007 Jeju, Korea, pp.53-56.
[28] L. Menager, M. Soueidan, B. Allard, et al, *IEEE Transactions on Power Electronics* (2010), 25(7) 1667-1671.
[29] E. Vagnon, P.O. Jeannin, J.C. Crébier, et al, *IEEE Transactions on Industry Applications*(2010), 46(5), 2046-2055.
[30] Uwe Scheuermann, in *Proceedings of 7th International Conference on Integrated Power Electronics Systems*, March 6-8, 2012, Nuremberg, Germany, pp. 464-471.
[31] A. A. Wereszczak, D. J. Vuono, Z. Liang, in *Proceedings of 7th International Conference on Integrated Power Electronics Systems*, March 6-8, 2012, Nuremberg, Germany, pp. 451-456.
[32] J.F. Li, C.M. Johnson, C. Buttay, S. Wissam, S. Azzopardi, Bonding strength of multiple SiC die attachment prepared with sintering of Ag nanoparticles, Submitted to *IEEE Transactions on Components, Packaging and Manufacturing Technology*.
[33] J.F. Li, I. Yaqub, M. Corfield, P.A. Agyakwa, C.M. Mark Johnson, Comparison of thermo-mechanical reliability of high-temperature bonding materials for attachment of SiC devices, Accepted by *8th International Conference on Integrated Power Electronics Systems*, February 25-27, 2014, Nuremberg, Germany.